The 9th European Congress on Computational Methods in Applied Sciences and Engineering
ECCOMAS Congress 2024
3–7 June 2024, Lisboa, Portugal

TOWARDS AN ACTUATOR LINE REPRESENTATION OF THE YARN INSERTION PHASE IN AIR-JET WEAVING

AXEL BRAL[1], LODE DAELEMANS[2] AND JORIS DEGROOTE[1,3]

[1] Department of Electromechanical, Systems and Metal Engineering
Ghent University
Sint-Pietersnieuwstraat 41-B4, 9000 Ghent, Belgium
e-mail: Axel.Bral@UGent.be

[2] Department of Materials, Textiles and Chemical Engineering (MaTCh)
Ghent University
Technologiepark Zwijnaarde 70, 9052 Zwijnaarde, Belgium

[3] Flanders Make @ UGent - Core lab MIRO
9000 Ghent, Belgium

Key words: Actuator Line Method (ALM), Computational Fluid Dynamics (CFD), yarn, multiscale analysis

Summary. Air-jet weaving is known for allowing high production rates, however at the cost of an increased energy demand. State-of-the-art techniques to simulate these processes where a yarn interacts with high-speed air flow are however far from mature to reliably account for the often hairy surface structure of the yarn. This contribution develops an actuator line representation of the yarn where the hairy details of the yarn are not resolved in the machine scale simulations but are accounted for by the use of precomputed aerodynamic force coefficients. However, as actuator line methods were originally developed to represent wind turbine blades, some important changes are necessary. These include (i) the alternative formulation of orientation of the yarn with respect to the flow, (ii) the use of continuous 2D force distribution kernels, instead of the classic 3D spherical Gaussian kernels at the actuator points and, (iii) the location at which the velocity is sampled. With these changes, it is possible to represent a hairy yarn in a machine scale simulation at a much lower computational cost than would be the case for fiber-resolved simulations.

1 INTRODUCTION

Air-yarn interactions are the heart of air-jet weaving machines, allowing for high insertion rates (up to 2000 per minute) and low maintenance costs. However, this comes at the cost of an increased energy demand (in the order of 5 kWh/kg of woven fabric) when compared to other weaving techniques such as rapier or shuttle weaving [1]. Attempts to reduce the energy use of air-jet weaving looms are mostly limited by the weaving stability, which is determined by the interactions between the weft yarn and air jets. Currently, these interactions are not yet well understood. Numerical models that are capable of accounting for these interactions are therefore a welcome and useful tool.

State-of-the-art simulation techniques that are considering a complete fluid-structure interaction (FSI) model, usually represent the yarn as a smooth and solid cylinder [2]. In reality

however, multifilament yarns are used due to their increased weavability compared to monofilament yarns. This is caused by larger aerodynamic forces as a consequence of their irregular and hairy surface appearance. Capturing these details of the yarn surface structure in a machine-scale simulation is currently not feasible. Indeed, roughly 97 million cells are needed to discretize the flow domain around a yarn segment with a length of only 2.25 mm in a wall-resolved computational fluid dynamics (CFD) simulation on the level of the fibers [3]. Upscaling this domain towards a machine length of the order of 2 m is computationally too demanding.

It is clear that resolving the viscous boundary layer at the fiber scale on the flow side of an FSI model is not realistic for a machine scale simulation. However, there exist alternatives to incorporate complex and slender structures in fluid flows. Peskin [4] developed an immersed boundary method (IBM) to simulate the motion of heart valves in viscous incompressible flow. In this framework, the kinematic coupling is enforced. That is, the velocities of the fluid and the structure are equal at the location of the valve. The reaction force of the structure on the fluid is incorporated in the flow domain using a diffuse source term. Due to the spatial spreading of this source term, the interface is not sharply resolved and thus allows allows for cell sizes in the fluid mesh that are larger than the thickness of the structure, a property that is desirable for the intended application. This type of IBM has been successfully used to simulate global 3D flow over 1D slender beams [5]. A downside of these models is that the reaction force of the structure on the flow is computed in the structural model. As a consequence, the complex yarn geometry and its structural properties should be modelled with great accuracy.

As alternative to the diffuse boundary IBM above, there also exist sharp-interface IBMs which can be subdivided in two classes. On one side, there is the ghost-cell methodology [6, 7] for both compressible and incompressible flows. The sharp representation of the interface is taken care of by reconstructing the no-slip condition at the fluid-solid interface through the use of so-called ghost cells that overlap with the solid object. On the other side, there is the cut-cell methodology [8] where the fluid-structure interface divides cells in a fluid and a solid part. The wall boundary conditions are then applied at the newly created cell faces. Overall, these sharp-interface IBMs require a proper resolution of the boundary layer around the object since the forces at the interface are computed from the flow field (i.e. the pressure and wall shear stress). For multifilament yarns, this would then lead to an excessive cell count, even more than in the wall-resolved simulations of a yarn segment using the overset mesh technique in Bral et al. [3].

The IBMs described above are not suited for the simulation of a yarn insertion phase in air-jet weaving as they do not completely alleviate the need for a microscale description of the yarn in the macroscale machine simulation. However, the diffuse character of the original IBM formulation is an interesting property since it allows for coarser fluid meshes, which drastically reduces the computational cost. Ideally, the forces at the fluid-solid interface can be incorporated in the momentum sources without having to resort to high-fidelity descriptions of the yarn geometry at the structural level, such as in Bral et al. [9].

In wind energy engineering, such type of methodology has been developed in the past decades: the actuator line method (ALM) [10]. The aerodynamic forces are reconstructed along the windturbine blades (that are represented each as a line of actuator points) using the local flow velocities and tabulated airfoil data, i.e. drag and lift force coefficients. The reaction forces of the airfoil are added as source terms to the momentum equation of the flow in these actuator points, with spatial smearing to avoid singularities. As such, it is possible to use coarse meshes compared to the blade chord length. Troldborg et al. [11] resolved the rotor radius within 30

mesh cells while still capturing the main flow features in the far field wake (> 1 rotor diameter away from the wind turbine). This in turn allows to simulate wake interactions occurring in wind farms in a computationally efficient manner since there is no longer the need to resolve the flow at the blade surface. Additionally, the fluid-structure interface is now reduced to a line of points, allowing for a straightforward coupling to a beam-like representation of the blade on the structural side of the FSI model.

Despite the aforementioned advantages, there are also some disadvantages to the original implementation of the ALM [10] that prohibit direct use of this technique to simulate yarns in air-jet weaving machines. First, in wind turbine applications, the lift force usually dominates the drag force. Hence, the resulting force vector is nearly perpendicular to the local velocity vector in the actuator points. As a consequence, the magnitude of the velocity vector at the actuator point is not greatly influenced by the momentum sources. In contrast, the yarn under consideration in Bral et al. [3] only experiences drag forces, having a significant parallel component to the velocity vector and in opposite direction. The local relative velocity magnitude at the actuator points is as such influenced by the momentum sources and is no longer a reasonable approximation of the undisturbed relative velocity for which the force coefficients are derived. Moreover, the concept of angle of attack should be adapted, since now the angle between the local relative flow velocity vector and the yarn tangent vector at the actuator point are of interest rather than the orientation of the relative flow with respect to the chord. The latter concept has been implemented in a 2D axisymmetric representation of the flow field in the main nozzle of an air-jet weaving loom in Osman et al. [12]. In this implementation, the aerodynamic forces are uniformly spread out in the radial direction.

The current contribution develops a 3D actuator line model of a hairy yarn during the weft insertion phase in air-jet weaving. This allows for computationally more feasible FSI simulations on the machine scale since the individual fibers do not longer need to be resolved. Yet, the hairy nature of the yarn is accounted for in the force coefficients, which are derived in our previous work [3]. The method is then tested on a stationary yarn in the main nozzle of an air-jet weaving loom.

2 METHODOLOGY

The ALM represents an object, typically a windturbine blade, as a set of actuator points along its (aerodynamic) centerline. In these actuator points, the aerodynamic forces are computed from the local relative velocity and predetermined aerodynamic force coefficients. These forces are subsequently introduced in the computational domain by the use of momentum source terms. To avoid singularities, these sources are smeared out in space around the actuator points using a so-called regularization kernel. In this way, the ALM is comparable to the diffuse IBM described in the previous section, but the aerodynamic forces are computed from tabulated data instead of as structural reaction forces caused by an imposed displacement. This implies that the kinematic coupling is not enforced at the fluid-structure interface. As a consequence, there is no direct need for a geometrically complex structural model.

The current contribution tailors the initial version of the ALM, developed by Sørensen and Shen [10], to simulate a wool fiber yarn of 28.8 tex [g/1000m]. Only the main adaptations of the current framework with respect to the initial version are highlighted below. The resulting framework is implemented in user-defined functions (UDFs) in ANSYS Fluent version 2023R1.

A first change is the concept of angle of attack being replaced by an angle θ indicating the angle between the local relative velocity and the yarn centerline at the considered actuator point. This change was already implemented in previous work by Osman et al. [12].

Secondly, the forces are introduced in the computational domain in a slightly different manner. In the original formulation of the ALM, a 3D spherical Gaussian kernel $\eta_{\epsilon,3D}$ with shape parameter ϵ is used to spread the forces around the actuator points:

$$\eta_{\epsilon,3D}(r) = \frac{1}{\epsilon^3 \pi^{3/2}} \exp(-(r/\epsilon)^2). \tag{1}$$

Herein, r is the distance between the actuator point and the mesh point at which the momentum source is applied. This means that the spacing between subsequent actuator points relative to ϵ is an important parameter as it determines the overlap between two neighbouring force spheres. Alternatively, Jha and Schmitz [13] developed an actuator curve formulation. Instead of spherical Gaussian kernels around the actuator points, a 2D Gaussian kernel is used in a continuous matter. The momentum source applied at cell center C_j is given by

$$\vec{F}_{C_j} = t\eta_{\epsilon,2D}(r)\vec{F}_{P_{a,i}} + (1-t)\eta_{\epsilon,2D}(r)\vec{F}_{P_{a,i+1}}, \tag{2}$$

with t the normalized tangential coordinate of C_j along line $P_{a,i}$-$P_{a,i+1}$ (or thus the actuator element E_i), r the radial distance of C_j to E_j and finally $\vec{F}_{P_{a,i}}$ is the linear force (in N/m) at actuator point $P_{a,i}$, see Figure 1. The 2D regularization kernel $\eta_{\epsilon,2D}$ then becomes

$$\eta_{\epsilon,2D}(r) = \frac{1}{\epsilon^2 \pi} \exp(-(r/\epsilon)^2). \tag{3}$$

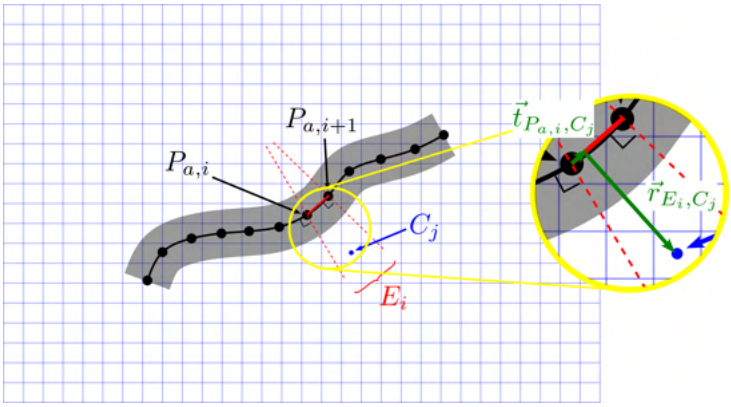

Figure 1: Schematic of the actuator curve concept. Cell center C_j belongs to actuator element E_i and the aerodynamic force obtained from linear interpolation of actuator points $P_{a,i}$ and $P_{a,i+1}$ is scaled with a 2D Gaussian kernel based on the radial distance r of C_j to the actuator element.

The third major change with respect to the standard ALM formulation concerns the location where the velocity is sampled. In the original formulation, the velocity sampling happens at the actuator points themselves. However, in the current application of yarns experiencing dominantly drag forces, the velocity magnitude near this location is affected by the presence of

the opposing momentum sources. As a consequence, the velocity sampled at the actuator points is by definition an underestimation of the free-flow velocity around the actuator line. For this reason, an upstream sampling strategy is adopted, see Figure 2.

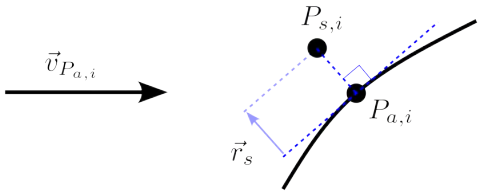

Figure 2: Location of velocity sampling point $P_{s,i}$ with respect to actuator point $P_{a,i}$ and the local relative velocity vector $\vec{v}_{P_{a,i}}$.

In a first step, the relative velocity $\vec{v}_{P_{a,i}}$ is sampled in the actuator point $P_{a,i}$ itself to estimate the flow direction. Usually, the actuator points do not coincide with the mesh point. Therefore, the velocity is interpolated from the mesh using a 3D Gaussian kernel η_{3D} centered around $P_{a,i}$. The relative velocity of the flow with respect to $P_{a,i}$ is considered by incorporating the yarn motion. Secondly, $\vec{v}_{P_{a,i}}$ is projected on a plane normal to the yarn centerline at this actuator point, and as such the vector $\vec{r}_s$ in Figure 2 is obtained. The sampling point $P_{s,i}$ is located at a distance equal to the yarn diameter upstream of $P_{a,i}$, along $\vec{r}_s$. Finally, the velocity is sampled at $P_{s,i}$ from the computational mesh using the interpolation weights from kernel η_{3D} centered around $P_{s,i}$. The weights of this 3D Gaussian kernel are normalized so that their sum is 1, irrespective of the mesh resolution.

When the flow is purely axial to the yarn, upstream sampling points as in Figure 2 are undefined. Therefore, a circle with radius equal to the yarn diameter is constructed around $P_{a,i}$ in a plane normal to the yarn centerline in $P_{a,i}$. The velocity is then obtained as the arithmetic mean of the velocity sampled in 5 equidistant points on this circle.

The velocity to reconstruct the aerodynamic forces at the actuator points is then a combination of the upstream sampled velocity and the circumferentially averaged velocity with weights $1-cos^{10}(\theta)$ and $cos^{10}(\theta)$, respectively. Here, the angle θ is the angle between the relative velocity $\vec{v}_{P_{a,i}}$ and the tangent vector to the yarn centerline in $P_{a,i}$.

It should be noted that the distance of one yarn diameter between actuator point and corresponding sampling points is design choice, here related to a physical dimension of the yarn under investigation. From the point of view of disturbing the flow field with the momentum sources, this distance should be as large as possible. In contrast, to account for the local flow characteristics around the actuator points, this distance should be minimized. Other researchers that include the tower and nacelle in an ALM formulation for horizontal axis wind turbines, also point out the difficulty of where exactly the velocity should be sampled in drag-dominated actuator lines [14].

3 RESULTS AND DISCUSSION

The adapted ALM framework is tested in two different cases. Firstly, the microscale CFD simulations of our previous work [3] are replicated, but with the yarn represented as an actuator line instead of the computationally expensive wall-resolving overset meshes. In this case, the ALM should be able to reproduce the forces presented in Bral et al. [3] while demanding less computational effort. Secondly, the framework is applied to a main nozzle of an air-jet weaving loom.

3.1 Replicating microscale forces

In a first step, the ability of the ALM framework to replicate the aerodynamic forces using the coefficients fitted from the wall-resolved simulations, is tested. A straight yarn segment of length 2.25 mm and with radius 177.31 μm is divided in 11 equally spaced actuator points along its axis and placed in a cubic domain with sides measuring 24.7 mm. The mesh is depicted in Figure 3: a coarse discretization with 6 cylindrical refinement layers that gradually halve the cell sizes down to 6 μm. This is the background mesh that is described in our previous work [3]. The inlet velocity ranges between 10 and 175 m/s and the orientation of the static yarn with respect to the inflow velocity varies from 0° (axial flow) to 90° (cross flow). Other simulation settings can be found in Bral et al. [3]. The remainder of this section explores the effect of the shape parameter ϵ of the regularization kernel $\eta_{\epsilon,2D}$ and the mesh size Δh on the resulting aerodynamic forces.

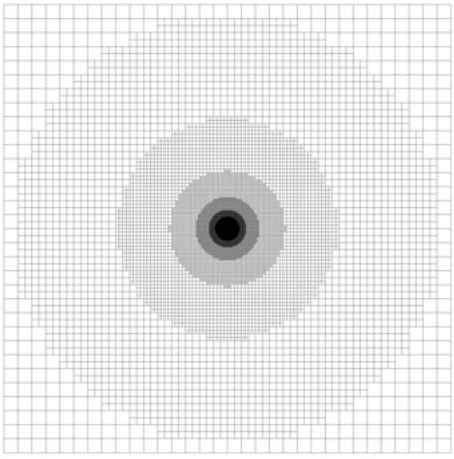

Figure 3: Cross-section of the mesh and visualization of the refinement layers. The innermost layer has a cell size Δh of 6 μm.

To explore the effect of the shape parameter ϵ, which ranges between 0.25 and 4 times the yarn radius, the inner three refinement layers of the mesh have been removed as to accelerate the simulations. This leads to a mesh size of about 1.2 million cells, a reduction with a factor of over 26 with respect to the mesh with all six refinement layers. Similarly to our previous work [3], the yarn end effects have been mitigated by ignoring the first and last 20 % of the yarn sample

length. Figure 4 shows the relative error of the calculated forces using ALM ($\vec{F}_{ALM}$), that is the integral of the forces over the actuator elements, and the aerodynamic force calculated using the velocity at the inlet ($\vec{F}_{fit}$) for a constant inflow velocity of 100 m/s. In essence, this is a measure for the error in sampled velocity compared to the inlet velocity, since the two mentioned ways to compute the forces rely on the same aerodynamic force coefficients.

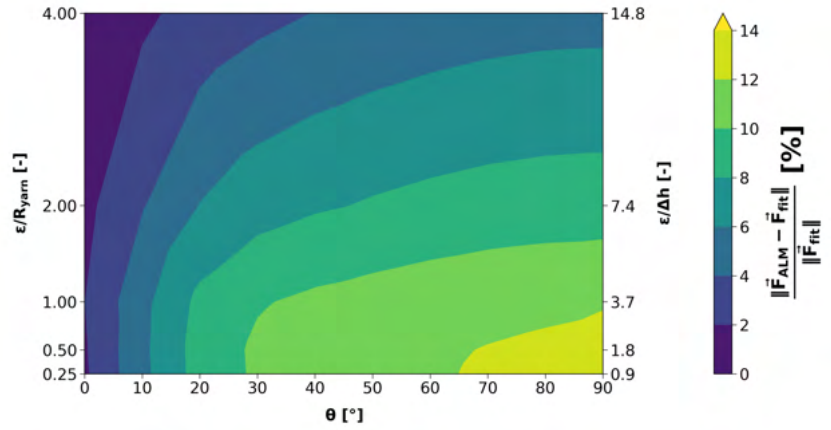

Figure 4: Relative error of aerodynamic forces computed at the actuator points and at the inlet for an inlet velocity of 100 m/s, varying yarn orientations and varying shape parameters ϵ. The latter is non-dimensionalized based on the yarn radius $\mathrm{R_{yarn}}$ on the left vertical axis and the cell size at the actuator points Δh on the right vertical axis.

This graph is similar for other inflow velocities, and it can be seen that the relative error maximizes for small regularization kernels and cross flow conditions. This can be explained using Figures 5 and 6, where the velocity profiles along the yarn for different kernel widths ϵ are shown alongside the velocity profile from the wall-resolved simulations (in black, with label 'overset'). The different columns denote different axial positions along the yarn, at $\pm 1 D_{yarn}$ from the yarn center point. The vertical axes at the top rows ('drag pos.') denote the position along the drag axis, that is along $\vec{r}_s$ in Figure 2 based on the global inflow direction. Here, the flow direction is from positive drag positions towards negative drag positions. Finally, the bottom rows ('lift pos.') denote the position along the lift axis, or perpendicular to the page in Figure 2. The red dotted lines in the top rows denote the position at which the velocity is sampled in the upstream sampling points $P_{s,i}$.

Figures 5 and 6 confirm that the kinematic coupling condition is not satisfied: the velocity in the ALM framework does not come to a standstill at the yarn surface, unlike in wall-resolved simulations. Additionally, the effect of the kernel width is visible only very locally. The smaller the kernel, the larger the peak value of the momentum source term and thus the lower the local velocity at the actuator elements. This explains the dependency of the velocity sampling error on the kernel width. However, the global flow features are not largely affected by this kernel width. Indeed, the difference is visible only within 6 yarn diameters from the yarn centerline in the wake of the yarn in cross flow, see the top row of Figure 6.

Secondly, for cross flow it can be seen that the sampling occurs in the upstream stagnation zone. Indeed, the flow velocity magnitude is already reduced even though for the smallest kernel

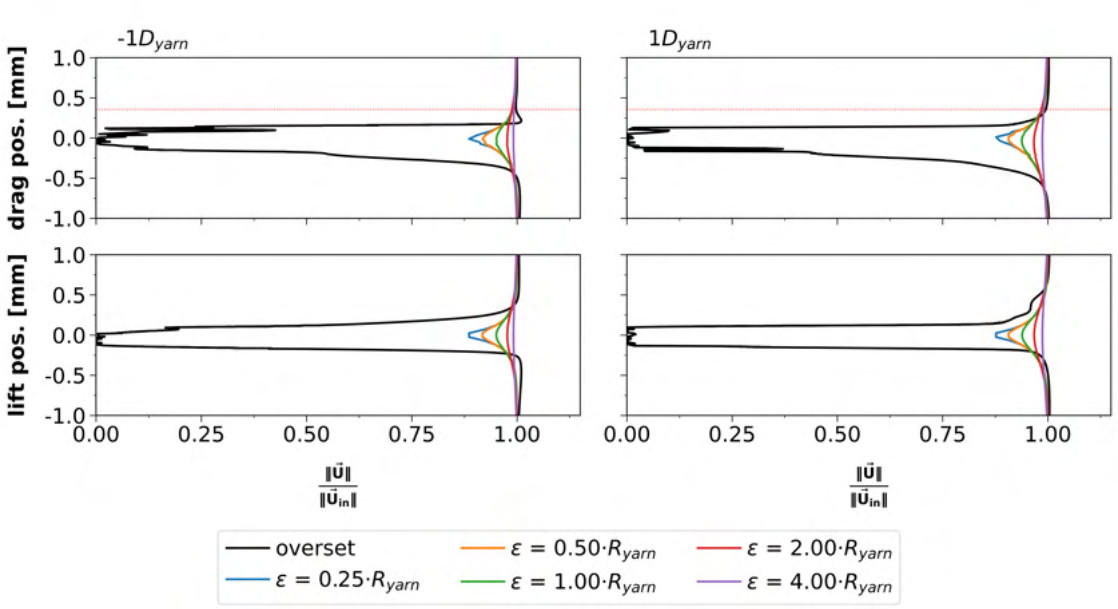

Figure 5: Profiles showing the velocity deficit along drag and lift unit directions at different axial positions of the yarn at an inlet velocity of 100 m/s and orientation $\theta = 10°$, which is nearly axial flow.

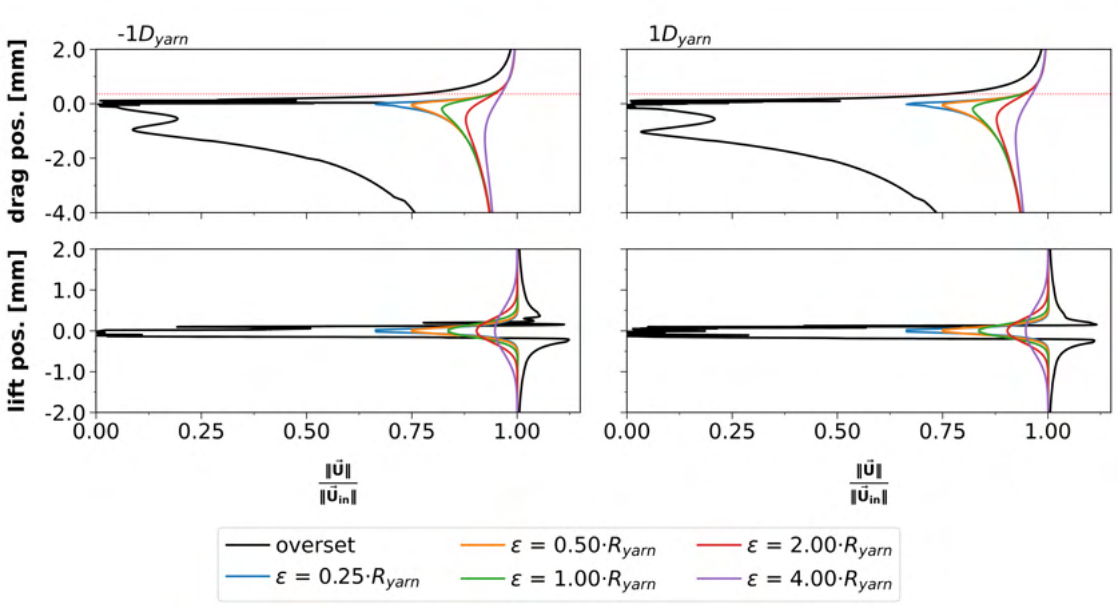

Figure 6: Profiles showing the velocity deficit along drag and lift unit directions at different axial positions of the yarn at an inlet velocity of 100 m/s and orientation $\theta = 90°$, which corresponds to cross flow conditions.

widths (0.25 R_{yarn} and 0.5 R_{yarn}), the magnitude of the momentum source term is negligible ($\ll 1$ % of the peak value). In contrast, for nearly axial flow no such stagnation zone exists and the sampling occurs outside of the boundary layer and in free-stream conditions. This explains the dependency of the error in aerodynamic forces on the orientation of the yarn with respect to the global flow direction. In air-jet weaving, the flow is mostly aligned with the yarn, with small perturbations caused by wave propagation in the yarn. As such, the local flow angles are rather low which in turn limits the velocity sampling error to an acceptable range. Moreover, the kernel size had a very limited impact on the sampling error in nearly axial flow conditions. In future work, this dependency of the kernel width ϵ and the orientation of the yarn on the calculation of aerodynamic forces could be incorporated in the force coefficients and as such reduce this error.

Finally, the influence of the mesh resolution has been tested in the conditions of an inflow velocity of 100 m/s and an angle of 20° between the centerline of the yarn and the inflow direction vector. Figure 7 shows the relative error of $\vec{F}_{ALM}$, the line integral of the forces computed at the actuator points using the trapezoid rule, and the volume integral of the momentum sources that are effectively applied in the computational domain, $\vec{F}_{vol}$. This is a measure of how much the mesh discretization influences the normalization of the regularization kernel. It follows that this discretization error is negligble, irrespective of the ratio $\epsilon/\Delta h$, except for the absence of refinement layers. This corresponds to an actuator element size $\|E_{a,i}\| = \|P_{a,i+1} - P_{a,i}\|$ that is larger than the cell size Δh, as $\|E_{a,i}\|/\Delta h$ equals 1.71 for zero refinement layers and 0.86 for one refinement layer. It can thus be concluded that the mesh size Δh should remain smaller than the actuator element size $\|E_{a,i}\|$ for the current implementation of the ALM.

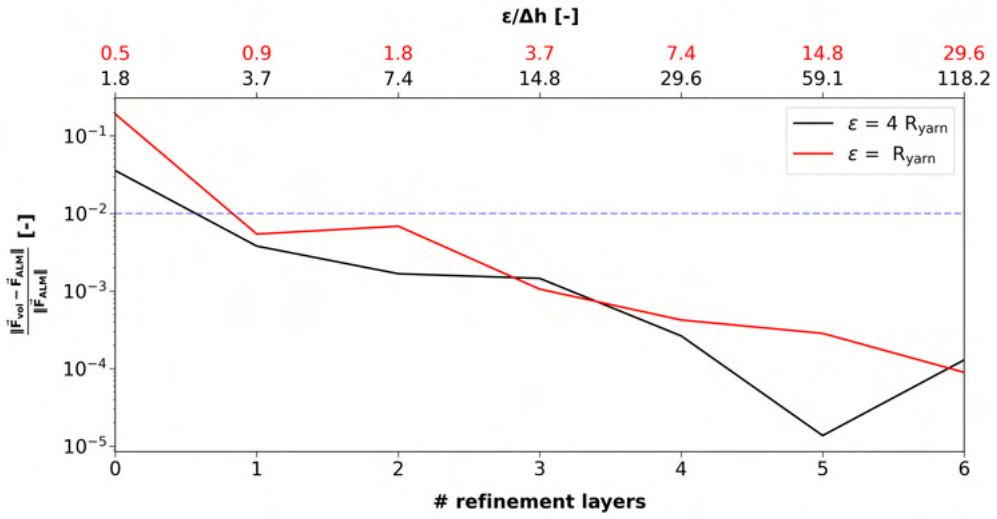

Figure 7: Relative error of the line integral of the aerodynamic forces computed at the actuator points and the volume integral of the momentum sources in the computational domain as function of the number of refinement layers. The upper horizontal labels $\epsilon/\Delta h$ relate the kernel size size to the size of the mesh cells for $\epsilon = 4R_{yarn}$ (in black) and $\epsilon = R_{yarn}$ (in red). The blue dashed line indicates a relative error of 1 %.

3.2 Stationary yarn in main nozzle

The next step is to apply the developed ALM to a larger domain, for example the main nozzle of an air-jet weaving loom. A yarn segment of length 0.283 m subdivided in 90 actuator elements was held at standstill along the centerline of the cylindrical main nozzle geometry and mesh described in Delcour et al. [2]. The inlet pressure is set to 5 bar gauge and the size of the regularization kernel ϵ is set equal to the yarn diameter (355 μm). Figure 8 shows the highly non-uniform axial velocity distribution throughout the main nozzle whereas Figure 9 depicts the axial momentum source, indicating a smooth distribution over the yarn axis owing to the actuator curve formulation.

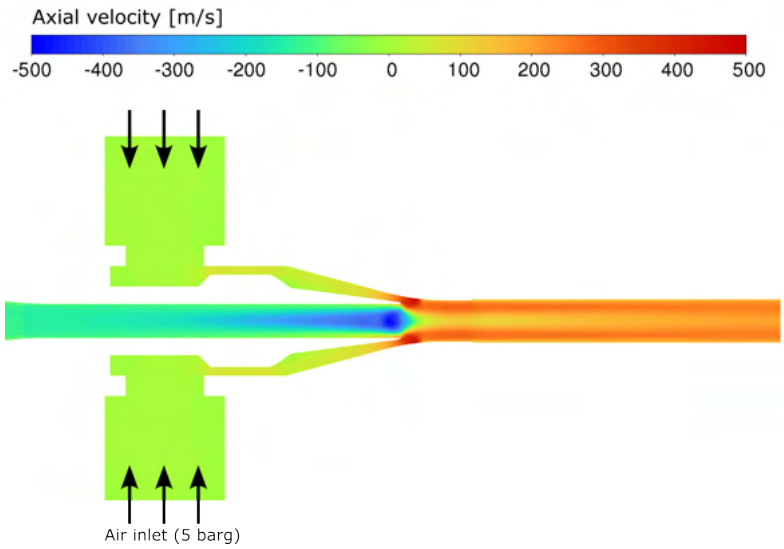

Figure 8: Contour of the axial (horizontal) velocity in the main nozzle. The domain and yarn segment continue beyond the image borders.

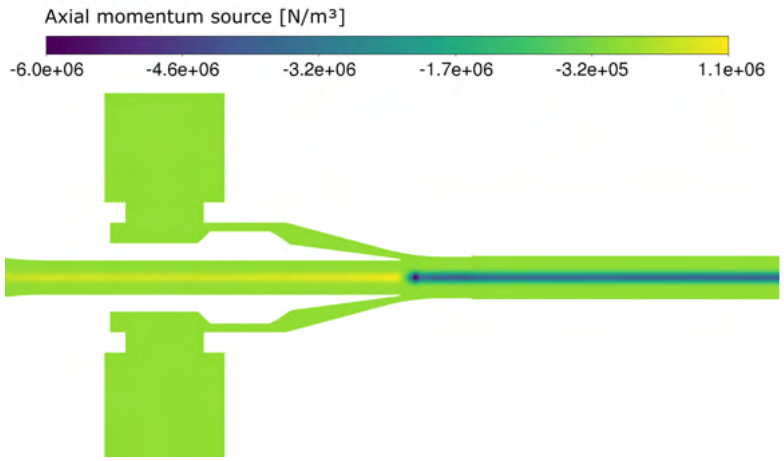

Figure 9: Contour of the axial (horizontal) momentum source in the main nozzle.

The presented ALM allows to efficiently incorporate the yarn's hairy surface structure in machine scale simulations. Indeed, the above steady-state calculation on a mesh of 1.2 M cells takes approximately 20 minutes on 4 nodes with 2 64-core AMD Epyc 7763 CPUs at 2.45 GHz. It is roughly estimated that a full wall-resolved simulation with the same nozzle geometry would take 3000 h $\approx$ 0.3 [h] $\cdot \frac{96.8e6 \text{ [cells]}}{1.2e6 \text{ [cells]}} \cdot \frac{0.283 \text{ [m]}}{0.00225 \text{ [m]}}$, which makes it impractical to scale it up further to a complete machine of approximately 2 meters long including multiple relay nozzles.

Future work involves coupling the presented ALM model for the flow to a lightweight structural model, where the yarn is represented as a chain of beam-like elements while still accounting for the microstructural properties as presented in Bral et al. [9].

4 CONCLUSION

This paper presents a methodology to efficiently and reliably represent a hairy yarn in large-scale computational fluid dynamic (CFD) simulations of textile manufacturing processes. This is accomplished by tailoring the actuator line method (ALM), initially developed for horizontal axis windturbines, to simulate drag-dominated objects such as yarns. The microscopic properties are accounted for in the aerodynamic force coefficients. With respect to the original formulation of the ALM, two major changes have been implemented. Firstly, the velocity sampling location is shifted more upstream to avoid interference of the sampled velocity with the momentum sources, which act in the parallel but opposite direction of the relative velocity vector in the actuator points. However, there is a trade-off between remaining in the local flow field of the actuator point and reducing the influence of the momentum sources. The presented ALM model has been tested with several kernel widths ϵ additional to the influence of the mesh resolution. It was found that the yarn orientation is the largest contributor to the error in sampled velocity with respect to free-stream conditions. In cross flow conditions, also the kernel size ϵ becomes an important parameter with a maximal error in pure cross flow with a narrow regularization kernel. When this methodology is applied to large scale applications, for example real-life weaving machines, the reduction in computational time is significant as the small flow scales do not need to be resolved anymore, yet are incorporated in the aerodynamic force coefficients. This is an important step towards coupled fluid-structure interaction (FSI) simulations of a hairy yarn insertion in air-jet weaving machines.

ACKNOWLEDGEMENTS

The computational resources and services used in this work were provided by the VSC (Flemish Supercomputer Center), funded by the Research Foundation Flanders (FWO) and the Flemish Government: department EWI.

FUNDING

The authors gratefully acknowledge the funding by the Research Foundation Flanders (FWO) with project number 1S30824N.

REFERENCES

[1] C. Grassi, A. Schröter, Y. Gloy and T. Gries. 2016. "Energy efficiency approach to reduce costs of ownership of air jet weaving." Int J Mater Metall Eng 10, no. 12:1444–1450.

[2] L. Delcour, J. Peeters and J. Degroote. 2020. "Three-dimensional fluid-structure interaction simulations of a yarn subjected to the main nozzle flow of an air-jet weaving loom using a Chimera technique." Tex Res J 90, no. 2:194–212.

[3] A. Bral, L. Daelemans and J. Degroote. 2024. "A method to determine local aerodynamic force coefficients from fiber-resolved 3D flow simulations around a staple fiber yarn." Multibody Syst Dyn.

[4] C.S. Peskin. 1972. "Flow patterns around heart valves: A numerical method." J Comput Phys 10, no. 2: 252–271.

[5] N. Hagmeyer, M. Mayr and A. Popp. 2024. "A fully coupled regularized mortar-type finite element approach for embedding one-dimensional fibers into three-dimensional fluid flow." Int J Numer Methods Eng 125, no. 8:e7435.

[6] R. Ghias, R. Mittal and H. Dong. 2007. "A sharp interface immersed boundary method for compressible viscous flows." J Comput Phys 225, no. 1:528–553.

[7] R. Mittal, H. Dong, Bozkurttas M., et al. 2008. "A versatile sharp interface immersed boundary method for incompressible flows with complex boundaries." J Comput Phys 227, no. 10:4825–4852.

[8] J.H. Seo and R. Mittal. 2011. "A sharp-interface immersed boundary method with improved mass conservation and reduced spurious pressure oscillations." J Comput Phys 230, no. 19:7347-7363.

[9] A. Bral, L. Daelemans and J. Degroote. 2023. "A novel technique to simulate and characterize yarn mechanical behavior based on a geometrical fiber model extracted from micro-computed tomography imaging." Tex Res J 93, no. 9-10:2042–2062.

[10] J.N. Sørensen and W.Z. Shen. 2002. "Numerical Modeling of Wind Turbine Wakes." J Fluids Eng 124, no. 2:393–399.

[11] N. Troldborg, J.N. Sørensen and R. Mikkelsen. 2010. "Numerical simulations of wake characteristics of a wind turbine in uniform inflow." Wind Energy 13, no. 1:86–99.

[12] A. Osman, B. Malengier, S. De Meulemeester, et al. 2018. "Simulation of air flow–yarn interaction inside the main nozzle of an air jet loom." Tex Res J 88, no. 10:1173–1183.

[13] P.K. Jha and S. Schmitz. 2018. "Actuator curve embedding – an advanced actuator line model." J Fluid Mech 834:R2.

[14] M.J. Churchfield, S. Lee, S. Schmitz and Z. Wang. 2015. "Modeling Wind Turbine Tower and Nacelle Effects within an Actuator Line Model." In *33rd Wind Energy Symposium*.